In pursuit of structures in protoplanetary disks

By O. M. Umurhan

1. Motivation and objectives

This brief summarizes work devoted to studying the linear stability of baroclinic protoplanetary Keplerian disks. This work largely builds on the foundation and fundamental results obtained by Barranco, Marcus & Umurhan (2000) (hereafter BMU) which presented a model to describe structures in weakly baroclinic Keplerian disks.

Interest in protoplanetary disks has grown since the discovery of the first of what are now dozens of extrasolar planets around F and G type stars (Marcy 1996, Perryman 2000). The apparent ubiquity of planets suggests that the nebular disks (or *protoplanetary disks*), out of which these stars are born, must be susceptible to the development of structures. However, theoretical work (see references in BMU) argues that purely pressure-supported gaseous barotropic Keplerian disks do not undergo any known type of hydrodynamic instabilities. The basis for this claim is that the strong rotation in Keplerian shear flows manages to suppress any of the usual instabilities seen in laboratory shear flows such as the Taylor-Couette and Kelvin-Helmholtz instabilities (Drazin & Reid, 1982). Some investigators (*e.g.* Shu *et al.*, 1993) have gone so far as to claim that protoplanetary disks are featureless objects totally bereft of vortical structures or long-lasting stable patterns.

To counter this assertion, some investigators have suggested that the protoplanetary disk is sufficiently magnetized to undergo a magneto-rotational instability as first explored by Chandresekhar (1956) using linear analysis and later demonstrated numerically by Balbus, Hawley & Stone (1996) for fully nonlinear flows. However, Desch (2000) has indicated that disks suspected to be around solar type stars will be too cool and weakly ionized such that local dust particles in short time will sweep up the ionization in the gas, leaving the fluid nearly neutral. What little ionization is left in the disk is too little to allow strong coupling to an external magnetic field. Thus this mechanism is unlikely to play an important role in the formation of planets at the radii where the large gas giants are observed to reside.

The point of view taken by BMU is that a weakly baroclinic Keplerian disk will produce the type of shear flow that will promote hydrodynamical instabilities. The assumption was that the added component of vertical shear driven by baroclinic effects generates coherent structures in an otherwise featureless protoplanetary disk. To isolate this effect they derived a number of asymptotic reductions of the 3D Euler equations in cylindrical geometry with a central mass source. The work here outlines the linear theory of these reduced equations in order to:

- Study and determine the conditions for which waves in these baroclinic disks are unstable in order to develop a physical intuition of the instability process.
- Provide analytical results to test the numerical techniques to be used in simulating the fully three dimensional Euler equations on a section of the protoplanetary disk.

Ongoing collaborative work with P. Marcus and J. Barranco is exploring the proposition that disk baroclinicity may be sufficient to generate structures. This work is being

done mainly through the development and implementation of fully three-dimensional simulations of the reduced 3D Euler equations derived in BMU.

The second half of this brief is concerned with work done with N. J. Balmforth and C. Picollo at the University of California, Santa Cruz, concerning the problem of characterizing the development of vortical structures in two-dimensional shearing flows in a planetary-scale vorticity field.

2. Physical considerations, the reduced equations, and linear theory

A baroclinic disk is an equilibrated pressure-supported gaseous disk with a central gravitational source in which the pressure and density iso-lines do not align. The physical cause for such a misalignment is most likely the uneven penetration, absorption, and heating of the gas by radiation coming from the central star. For a cylindrical geometry, *barotropic* pressure-supported Keplerian disks have azimuthal velocities that, though they are sheared strongly in the radial direction, have no variation of their speeds in the disk vertical direction. However, with only the most conservative assumptions for the baroclinic heating of the steady disk, it was shown in BMU that there will be a slight vertical shear of the azimuthal velocity. This result establishes the setting for what follows.

The asymptotic reduction of the full three-dimensional Euler equations have a number of physical assumptions built into them. First, that the disk is so cold that its vertical scale height is much smaller than its radial extent. Second, that dynamical structures (if they exist) appear in the baroclinic disk as small amplitude departures atop an otherwise featureless medium. Third, that coherent vortex structures of interest should be subsonic in the reference frame moving with respect to the vortex center. This last requirement provides additional constraints on the length and time scales to be explored within the 3D Euler equations. Since the rotation and shear in Keplerian disks are of comparable strengths, to hunt for vortex structures that are both subsonic and coherent means one must explore length scales that are small in the disk radial direction compared to the azimuthal and vertical directions. The picture is not of shallow structures in a thin disk, but rather of deep radially thin structures instead.

We investigate only two of the three sets of reduced asymptotics in BMU. The equations presented below are in non-dimensional form using the scalings assumed in BMU. In short, the velocities were scaled according to the local Mach number (ϵ). The sound speed is defined by

$$c_s^2 = \bar{P}(R_0, 0)/\bar{\rho}(R_0, 0), \tag{2.1}$$

where $\bar{P}(R_0, 0)$ and $\bar{\rho}(R_0, 0)$ are the pressure and density values at the disk midplane at a reference radial position R_0. The velocity is given by

$$v_{scale} = \Omega L_r \qquad \Omega = \sqrt{GM/R_0}, \qquad \epsilon = v_{scale}/c_s$$

where Ω is the local Keplerian rotation frequency at R_0 given by the mass of the central object, M. L_r is the radial length scale assumed of the vortical structure. Time is scaled to reflect the advective times for the disturbances. L_r is chosen so that the difference of the radial Keplerian speed across that length is the same order of magnitude as the velocity disturbances themselves. For notational convenience the equations are expressed in terms of momentum density, or $u = \bar{\rho}v$, where $\bar{\rho}$ is the steady-state disk density evaluated at the radial position R_0. The reduction procedure involves the *local* Cartesionization of the

cylindrical disk: in the resulting units x represents the disk azimuthal direction, y is the radial direction and, z denotes the vertical.

In the limit where the radial, azimuthal, and vertical disturbance scales are of equal magnitude but much smaller (as measured by the Mach number ϵ) than the scale of variations of the vertical component of the disk shear or the vertical disk gravity, we find the following equations,

$$\frac{\partial u_x}{\partial t} = -\nabla \cdot \left(\frac{\mathbf{u} u_x}{\bar{\rho}(R_0, z)} \right) + 2u_y - \frac{\partial \tilde{P}}{\partial x} \tag{2.2}$$

$$\frac{\partial u_y}{\partial t} = -\nabla \cdot \left(\frac{\mathbf{u} u_y}{\bar{\rho}(R_0, z)} \right) - 2\Big((u_x - \bar{\rho}(R_0, z)(3y/2 + \epsilon^2 \beta z^2) \Big) - \frac{\partial \tilde{P}}{\partial y} \tag{2.3}$$

$$\frac{\partial u_z}{\partial t} = -\nabla \cdot \left(\frac{\mathbf{u} u_z}{\bar{\rho}(R_0, z)} \right) - \frac{\partial \tilde{P}}{\partial z} - \epsilon^2 \tilde{\rho} z \tag{2.4}$$

$$0 = \nabla \cdot \mathbf{u}. \tag{2.5}$$

In BMU this reduced set was referred to as the *Round Vortices* equations. These reduced equations are anelastic owing to the assumed dominance of advection, thus sound waves are not present. Density and pressure, $\tilde{\rho}$ and $\tilde{P}$ respectively, represent their fluctuations from the steady disk state. The explicit appearance of z on the right-hand side of Eq. (2.4) represents the variable gravitational force as one moves vertically in the disk. The steady-state baroclinic Keplerian shear appears as a forcing term on the right-hand side of Eq. (2.3) because the reduction procedure that results in these equations involves subtracting the featureless disk from the full 3D Euler equations. On the length scales considered, the radial component of the Keplerian shear appears as a linear term in y while the baroclinic contribution appears as a term quadratic in z. The degree of baroclinicity is measured by the parameter β. We refer the reader for further details to BMU, § 3.

The other set of reduced equations we study assumes that the azimuthal and vertical extent of structures are of equal magnitude to the variations of the vertical shear and gravity but are much larger than the radial scale of the structures. These assumptions result in what is referred to in BMU as *Elongated Dynamics*:

$$\frac{\partial u_x}{\partial t} = -\nabla \cdot \left(\frac{\mathbf{u} u_x}{\bar{\rho}(R_0, z)} \right) + 2u_y - \frac{\partial \tilde{P}}{\partial x} \tag{2.6}$$

$$0 = -2\Big(u_x - \bar{\rho}(R_0, z)(3y/2 + \beta z^2) \Big) - \frac{\partial \tilde{P}}{\partial y} \tag{2.7}$$

$$\frac{\partial u_z}{\partial t} = -\nabla \cdot \left(\frac{\mathbf{u} u_z}{\bar{\rho}(R_0, z)} \right) - \frac{\partial \tilde{P}}{\partial z} - \tilde{\rho} z \tag{2.8}$$

$$\nabla \cdot \mathbf{u} = 0. \tag{2.9}$$

A notable difference between these equations and the ones presented before is that motion in the radial direction is entirely geostrophic, meaning that there is a constant balance between the Coriolis and pressure terms at all times during the flow.

In the following two subsections we explore the linear stability of these above two sets of equations. We do this using (a) standard channel flow boundary conditions and (b) periodic conditions in the "sliding box" coordinate system (Rogallo 1981).

2.1. *Round vortex linear theory*

We linearly perturb Eqs. (2.2)–(2.5) about the steady Keplerian state and write,

$$u_x = \bar{u}_x + u'_x \qquad u_z = 0 + u'_z \qquad u_y = 0 + u'_y \qquad \tilde{P} = \tilde{P}'. \tag{2.10}$$

For notational convenience we define $\bar{v}_x \equiv \bar{u}_x/\bar{\rho}(R_0, \epsilon z)$ so that in the unit scalings appropriate for Eqs. (2.2)–(2.5), the steady velocity shear appears as,

$$\bar{v}_x = 3y/2 + \beta\epsilon^2 z^2. \tag{2.11}$$

We assume that the disturbances are isothermal so that $\tilde{P}' = \bar{T}(R_0, \epsilon z)\tilde{\rho}'$ where $\bar{T}(R_0, \epsilon z)$ is the steady-state temperature profile evaluated at R_0, the radial position of the perturbation in cylindrical coordinates. We use the simplest form for $\bar{T}$: a constant plus local variations that are quadratic in ϵz. Linearizing Eqs. (2.2)–(2.5) gives,

$$\left(\frac{\partial}{\partial t} + \bar{v}_x\frac{\partial}{\partial x}\right) u'_x = -\frac{\partial \tilde{P}'}{\partial x} + \tfrac{1}{2}u'_y - 2\beta\epsilon^2 z u'_z \tag{2.12}$$

$$\left(\frac{\partial}{\partial t} + \bar{v}_x\frac{\partial}{\partial x}\right) u'_y = -\frac{\partial \tilde{P}'}{\partial y} - 2u'_x \tag{2.13}$$

$$\left(\frac{\partial}{\partial t} + \bar{v}_x\frac{\partial}{\partial x}\right) u'_z = -\frac{\partial \tilde{P}'}{\partial z} - \epsilon^2 z\tilde{P}' \tag{2.14}$$

$$\frac{\partial u'_x}{\partial x} + \frac{\partial v'_y}{\partial y} + \frac{\partial v'_z}{\partial z} = 0. \tag{2.15}$$

In the following we present results for the different boundary conditions of interest.

2.1.1. *Channel geometry*

In this section we look for solutions of the form $\exp i(\omega t + k_x x)$. For the boundary conditions at both the $\hat{z}$ and $\hat{y}$ boundaries we use,

$$\text{(i) } u'_z = 0 \text{ at } z = \pm\zeta \qquad \text{and} \qquad \text{(ii) } u'_y = 0 \text{ at } y = \pm 1, \tag{2.16}$$

which means no vertical flow at the top and bottom boundaries and no radial flow perturbations at the radial boundaries, $y = \pm 1$. For flexibility, we consider the the z boundary conditions at $\pm\zeta$ with ζ now a tunable parameter. We assume that β is an order 1 quantity and we write all quantities and solutions to Eqs. (2.12)–(2.15), including the frequency ω, as a perturbation series in powers of ϵ^2,

$$\tilde{P}' = \tilde{P}'_0 + \epsilon^2\tilde{P}'_2 + \cdots, \qquad u'_x = u'_{x0} + \epsilon^2 u'_{x2} + \cdots, \qquad \omega = \omega_0 + \epsilon^2\omega_2 + \cdots, \tag{2.17}$$

and similarly for u'_y and u'_z. We insert the expansion Eq. (2.17) into Eqs. (2.12)–(2.15) and collect like powers of of ϵ. At lowest order we combine equations and find,

$$(1-\psi^2)\left(k_x^2 - \frac{\partial^2}{\partial z^2}\right) u'_{y0} - \left(\psi^2\frac{\partial^2}{\partial y^2} - k_x^2\right) u'_{y0} = 0, \tag{2.18}$$

with $\psi = \omega_0 + \frac{3}{2}y$. Equation (2.18) is separable so we assume solutions of the form,

$$u'_{y0} = \Psi_\ell(y) Z_m(z). \tag{2.19}$$

Upon enforcing the no vertical flow boundary condition at $z = \pm\zeta$, we find that the vertical eigenfunctions $Z_m(z)$ are given by

$$Z_m(z) = \cos \pi n s f r a c z \zeta, \tag{2.20}$$

in which $m = (2n+1)/2$ where n is any integer. The solutions to Eq. (2.18) show that the $\Psi_\ell(y)$'s are a discrete infinite set of eigenfunctions (ordered by integer ℓ) composed of linear combinations of Bessel functions of the first and second kinds. The specific linear combinations are determined by imposing the boundary conditions at $y = \pm 1$. The lowest order frequencies are real and have been confirmed by numerical computations of the eigenvalue problem. Furthermore, the following orderings for ω_0 hold: $|\omega_0(\ell_1, k_x)| > |\omega_0(\ell_2, k_x)|$ for $|\ell_1| < |\ell_2|$.

In the long wave limit, $k_x \to 0$, the frequency reduces to,

$$\omega_0^2 = 4m^2/(\ell^2\zeta^2 + 4m^2), \tag{2.21}$$

while for short waves it is,

$$\lim_{k_x \to \pm\infty} \omega_0 = \mathrm{sgn}(k_x)\,|\tfrac{3}{2}k_x|\,, \tag{2.22}$$

Equation (2.22) implies that the mode frequencies for all ℓ cluster together around $\frac{3}{2}k_x$ for $|k_x| \gg 1$.

The effect of disk baroclinicity, which appears in the vertical shear term, shows up at the next expansion order. Carrying out the perturbation expansion to order ϵ^2 and demanding that the boundary conditions be satisfied reveals that the resulting frequency corrections are real, and this has been validated by numerical computations. Thus, the no-radial/no-vertical boundary conditions explored here shows no destabilizing tendency due to disk baroclinicity to this order in ϵ.

2.1.2. *Sliding box coordinates*

We consider here Eqs. (2.12)–(2.15) in a reference frame that moves with the x-direction mean motion. The following coordinate transformation achieves this aim,

$$x' = x + \frac{3}{2}yt \qquad t' = t \qquad y' = y \qquad z' = z, \tag{2.23}$$

where the primes in Eq. (2.23) represent the transformed coordinate. These "sliding box" coordinates have previously been used in studies of plane Couette and other shearing flows (Marcus & Press 1977, Rogallo 1981 and Korycansky 1992). Inserting the coordinate transformation Eq. (2.23) into Eqs. (2.12)–(2.15) and assuming periodic solutions in the x' and y' directions, *i.e.* $\sim \exp i(k_y' y' + k_x' x')$, results in,

$$\frac{\partial u_x'}{\partial t} = -ik_x\tilde{P}' + \tfrac{1}{2}u_y' - ik_x\beta\epsilon^2 z^2 u_x' - 2\beta\epsilon^2 u_z' \tag{2.24}$$

$$\frac{\partial u_y'}{\partial t} = -2u_y' - i(k_y - \tfrac{3}{2}k_x t)\tilde{P}' - ik_x\beta\epsilon^2 z^2 u_y' \tag{2.25}$$

$$\frac{\partial u_z'}{\partial t} = -\mathcal{L}\tilde{P}' - ik_x\beta\epsilon^2 z^2 u_z' \tag{2.26}$$

$$\begin{aligned} 0 = &\left(k_x^2 + (k_y - \tfrac{3}{2}k_x t)^2 - \frac{\partial}{\partial z}\mathcal{L}\right)\tilde{P}' - ik_x u_y' \\ &-2i(k_y - \tfrac{3}{2}k_x t)u_x' - 4ik_x\beta\epsilon^2 z^2 u_z', \end{aligned} \tag{2.27}$$

with $\mathcal{L} \equiv \partial/\partial z + \epsilon^2 z$. For notational ease we have dropped primes from the coordinates. We solve the resulting partial differential equations (now in t and z) subject to the boundary conditions that there be no vertical flow at $z = \pm\zeta$.

Series solutions for Eqs. (2.24)–(2.27) are sought in powers of ϵ^2, *i.e.*

$$u'_x = u'_{x0} + \epsilon^2 u'_{x2} + \cdots, \tag{2.28}$$

and similarly for the other fluid quantities. We insert these expansions into Eqs. (2.24)–(2.27) and collect like powers of ϵ. The resulting lowest order equations admit separable solutions of the form,

$$\begin{aligned} u'_{x0} = \hat{u}_{x0}(t)Z_m(z) \qquad & u'_{y0} = \hat{u}_{y0}(t)Z_m(z) \\ \tilde{P}'_0 = \hat{P}_0(t)Z_m(z) \qquad & u'_{z0} = \hat{u}_{z0}(t)(\partial Z_m(z)/\partial z). \end{aligned} \tag{2.29}$$

The vertical eigenfunction $Z_m(z)$ is the same one that appears in Eq. (2.20). After inserting Eq. (2.29) into the lowest order set of equations we find that we are faced with having to solve the result numerically. However, by a dominant balance argument (Bender & Orszag, 1999) we find the (numerically verified) long time behavior of the solutions to be,

$$\hat{u}_{x0} \sim a_0 \left|\tfrac{3}{2}k_x t - k_y\right|^{\chi_+} + b_0 \left|\tfrac{3}{2}k_x t - k_y\right|^{\chi_-} \qquad \text{for } |t| \gg \tfrac{2k_y}{3k_x}, \tag{2.30}$$

where a_0 and b_0 depend on the choice of initial conditions, and where,

$$\chi_\pm = -(1 \pm \nu)/2, \quad \nu = (1 - 16m^2/9k_x^2)^{\frac{1}{2}}. \tag{2.31}$$

We note that $\hat{u}_{z0}$ has the same long time behavior as $\hat{u}_{x0}$ (*i.e.* $\hat{u}_{z0} \sim \mathcal{O}(\hat{u}_{x0})$), while the long time behavior of the radial momentum term is $\hat{u}_{y0} \sim \mathcal{O}(\hat{u}_{x0}/t)$. We can see from the solution of Eq. (2.30) that all modes decay algebraically since $0 \leq Re(\nu) < 1$ for all values of m and k_x. Thus we conclude that the lowest order solution which describes disturbances of a barotropic disk show no linear instability.

By carrying the perturbation analysis out to order ϵ^2 introduces disk baroclinicity. By demanding that the next order perturbation quantities satisfy the requisite boundary condition at $z = \pm\zeta$, the following long time behavior (numerically verified) is,

$$u'_{x2}/Z(z) \sim \beta a_2 \left|\tfrac{3}{2}k_x t - k_y\right|^{1+\chi_+} + \beta b_2 \left|\tfrac{3}{2}k_x t - k_y\right|^{1+\chi_-} + \mathcal{O}\left(t^{\chi_+}, t^{\chi_-}\right), \tag{2.32}$$

where a_2, b_2 are constants that depend on the initial conditions. The long time trend for u'_{z2} has the same temporal form as Eq. (2.32). However, u'_{y2} is down by a power of t, viz. $u'_{y2} \sim \mathcal{O}(u'_{x2}/t)$.

Introducing disk baroclinicity predicts that modes should exhibit $t^{1/2}$ (for ν imaginary) and $t^{1/2\pm\nu/2}$ (for ν real) amplitude growth for $t \gg |2k_y/3k_x|$, showing that a baroclinic disk is indeed unstable. Strictly speaking, the perturbation analysis breaks down when $\beta\epsilon^2 t = \mathcal{O}(1)$ since the correction term (*e.g.* u'_{x2}) breaks its ordering and competes with the lowest order term u'_{x0}. This signifies that linear theory is no longer valid at that late time and that disk baroclinicity has introduced a dynamically active feature. It is interesting to note that since u'_{y2} is down by one power of t, the radial momentum correction term exhibits algebraic decay in the long time limit despite the other terms (*e.g.* u'_{x2}, u'_{z2}) exhibiting algebraic growth.

2.2. *Elongated theory*

We now linearly perturb Eqs. (2.6)–(2.9) about the steady Keplerian state just as in Eqs. (2.10). We wish to demonstrate some of the peculiarities of these "elongated" asymptotic equations by adopting a couple of simplifications: disk baroclinicity is turned off ($\beta = 0$), and we assume no density fluctuations $\tilde{\rho} = 0$. In this limit the steady velocity

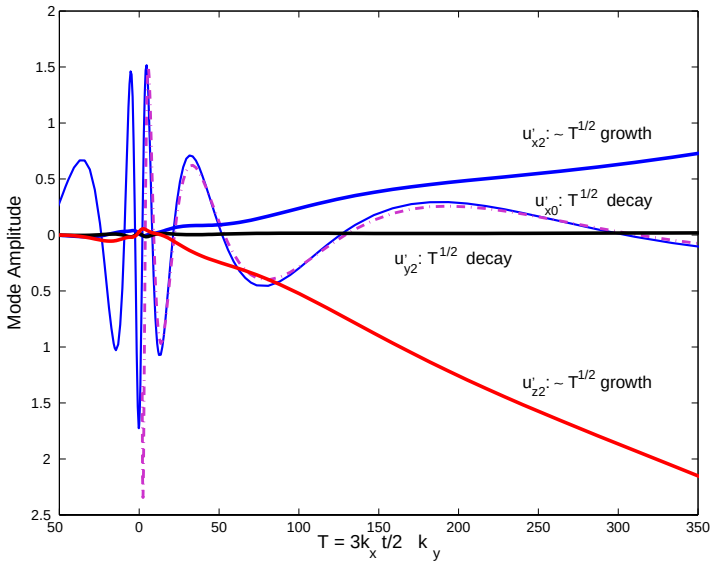

FIGURE 1. Mode evolution for the Round Vortices asymptotics in the sliding box coordinate frame. Shown here is the numerical evolution of a representative mode: $k_x = 1$ $k_y = 30$. The baroclinic effect, introduced here as a correction term in the analysis, predicts $t^{1/2}$ growth for the u'_x and u'_z velocity components corrections. The u'_y correction exhibits $t^{-1/2}$ decay. Also shown is the lowest order u'_x velocity together with the dominant balance result (—·—).

appears as $\bar{v}_x = 3y/2$. The linearized equations become,

$$\left(\frac{\partial}{\partial t} + \bar{v}_x \frac{\partial}{\partial x}\right) u'_x = -\frac{\partial \tilde{P}'}{\partial x} + \tfrac{1}{2} u'_y \tag{2.33}$$

$$0 = -\frac{\partial \tilde{P}'}{\partial y} - 2u'_x \tag{2.34}$$

$$\left(\frac{\partial}{\partial t} + \bar{v}_x \frac{\partial}{\partial z}\right) u'_z = -\frac{\partial \tilde{P}'}{\partial z} \tag{2.35}$$

$$0 = \frac{\partial u'_x}{\partial x} + \frac{\partial u'_y}{\partial y} + \frac{\partial u'_z}{\partial z}. \tag{2.36}$$

2.2.1. *Channel geometry*

We adopt the same periodic solutions and channel flow boundary conditions as in §2.1.1. Equations (2.33)–(2.36) may be combined into a single equation for the perturbation pressure,

$$-\left(\omega + \tfrac{3}{2} k_x y\right)^2 \frac{\partial^2 \tilde{P}'}{\partial y^2} + \frac{\partial^2 \tilde{P}'}{\partial z^2} = 0. \tag{2.37}$$

The following relationships hold between the pressure perturbation and the other fluid quantities,

$$u'_x = \frac{1}{2} \frac{\partial \tilde{P}}{\partial y} \quad , \quad u'_y = -i \left(\omega + \tfrac{3}{2} k_x y\right) \frac{\partial \tilde{P}}{\partial y} + 2 i k_x \tilde{P}'. \tag{2.38}$$

Since Eq. (2.37) is in separable form, we adopt the following ansatz,

$$\tilde{P}' = \Psi_{m\ell}(y) Z_m(z). \tag{2.39}$$

Enforcing the no vertical flow boundary condition reveals that the vertical structure function $Z_m(z)$ is the same one appearing in Eq. (2.20). The solution for $\Psi_{m\ell}$ is given by

$$\Psi_{m\ell} = \left(\frac{\omega_{m\ell} + \frac{3}{2}k_x y}{\omega_{m\ell} - \frac{3}{2}k_x}\right)^{\frac{1}{2}+i\frac{1}{2}\Delta} + \left(\frac{5+3i\Delta}{5-3i\Delta}\right)\left(\frac{\omega_{m\ell} + \frac{3}{2}k_x y}{\omega_{m\ell} - \frac{3}{2}k_x}\right)^{\frac{1}{2}-i\frac{1}{2}\Delta}, \tag{2.40}$$

$$\Delta = \left(\frac{16\pi^2 m^2}{9\zeta^2 k_x^2} - 1\right)^{\frac{1}{2}} \tag{2.41}$$

where ℓ is any non-zero integer.

Stability of the eigenvalues $\omega_{m\ell}$ depend on the sign of the expression appearing under the square root in Eq. (2.41),

$$\omega_{m\ell} = \tfrac{3}{2}k_x \coth\left(\tfrac{\ell\pi}{\Delta}\right), \qquad \text{for} \;\; 16\pi^2 m^2 - 9\zeta^2 k_x^2 > 0 \tag{2.42}$$

$$\omega_{m\ell} = -i\tfrac{3}{2}k_x \cot\left(\tfrac{\ell\pi}{\delta}\right), \qquad \text{for} \;\; 16\pi^2 m^2 - 9\zeta^2 k_x^2 < 0, \tag{2.43}$$

where $\delta = i\Delta$. Clearly, the situation in which $16\pi^2 m^2 - 9\zeta^2 k_x^2 < 0$ corresponds to waves that exhibit exponential growth. Thus, modes are unstable when both $|m| < 3\zeta|k_x|/4\pi$ and

$$\begin{aligned} &0 < \mathrm{mod}_\pi(\ell\pi/\delta) < \pi/2 \qquad &&\text{for} k_x > 0 \\ &\pi/2 < \mathrm{mod}_\pi(\ell\pi/\delta) < \pi \qquad &&\text{for} k_x < 0. \end{aligned} \tag{2.44}$$

2.2.2. *Sliding box coordinates*

We adopt the same coordinate transformations of Eq. (2.23) and the same solution form and flow boundary-initial conditions as was done in §2.1.2. Inserting the transformations into Eqs. (2.33)–(2.36) results in the following linear equations of motion,

$$\frac{\partial u_x'}{\partial t} = -ik_x P + \tfrac{1}{2}u_y' \tag{2.45}$$

$$0 = -2u_x' - i(k_y - \tfrac{3}{2}k_x t)\tilde{P}' \tag{2.46}$$

$$\frac{\partial u_x'}{\partial t} = -\frac{\partial}{\partial z}\tilde{P}' \tag{2.47}$$

$$0 = ik_x u_x' + i(k_y - \tfrac{3}{2}k_x t)u_y' + \frac{\partial}{\partial z}u_z'. \tag{2.48}$$

Since Eqs. (2.45)–(2.48) are autonomous in z, their solutions may be written in separable form (in t and z),

$$u_x' = \hat{u}_x(t)Z_m(z) \qquad u_y' = \hat{u}_y(t)Z_m(z) \qquad \tilde{P}' = \hat{P}(t)Z_m(z) \qquad u_z' = \hat{u}_z(t)(\partial Z_m(z)/\partial z), \tag{2.49}$$

and the vertical eigenfunctions $Z_m(z)$ are the same ones that appear in Eq. (2.20).

Inserting Eq. (2.49) into Eqs. (2.45)–(2.48) and subsequent simplification results in,

$$\tfrac{9}{4}k_x^2 \frac{\partial}{\partial T}\left(2T + T^2\frac{\partial}{\partial T}\right)\hat{P} + \frac{4\pi^2 m^2}{\zeta^2}\hat{P} = 0, \qquad T \equiv \tfrac{3}{2}k_x t - k_y. \tag{2.50}$$

Exact solutions to Eq. (2.50) are,

$$\hat{P} = a\left(\tfrac{3}{2}k_x t - k_y\right)^{\chi_+} + b\left(\tfrac{3}{2}k_x t - k_y\right)^{\chi_-} \qquad \chi_\pm = -\frac{3 \pm \nu}{2}\,,\ \nu = \left(1 - \frac{16m^2\pi^2}{9\zeta^2 k_x^2}\right)^{\frac{1}{2}}\,. \quad (2.51)$$

where a and b in Eq. (2.51) depend on the initial condition for that mode. The solution predicts that all perturbations in which $k_y k_x > 0$ will experience an algebraic singularity at $t_{\rm sing} = 2k_y/3k_x$ while those modes in which $k_y k_x < 0$ exhibit algebraic decay as $t \to \infty$. This means that adopting sliding box coordinates to describe the stability of these elongated dynamics predicts some rather curious stability properties. This suggests that our analysis of the reduced equations is highly sensitive to the boundary conditions that we adopt. Consequently, future work must answer the question as to which or what are the most physically appropriate boundary conditions to use in protoplanetary disk simulations.

Additionally, the algebraic singularity in the sliding box coordinates suggests that the elongated dynamics equations may have only limited applicability. The singularity at $t_{\rm sing}$ is not physical since, in the vicinity of $t_{\rm sing}$, the temporal scalings that led to Eqs. (2.6)–(2.9) break down as the perturbation time scale becomes very short,

$$\frac{\partial}{\partial t} \sim \mathcal{O}\left(\frac{1}{\Delta t}\right), \qquad \text{as} \quad t \to t_{\rm sing}, \quad (2.52)$$

in which, $\Delta t = t_{\rm sing} - t$. In other words, in this regime the time scales are no longer the advective ones that we assumed in deriving the asymptotic equations. Thus, the total time derivative term that is missing from Eq. (2.7) will become the same order of magnitude as the other terms in that equation when $\Delta t \sim \mathcal{O}(\epsilon)$, and ignoring this will lead to erroneous conclusions. Further analysis of this matter is needed.

2.3. *Discussion*

The asymptotic equations for each qualitative regime (*i.e.* round vortices or elongated dynamics) predict instabilities of some type. The elongated dynamics analysis predicts that there will be rather violent instabilities if one considers disturbances from the vantage point of the sliding box coordinate frame. As was discussed before, we do not expect the instability to be as violent as the results predict, primarily because the asymptotic equations begin to lose their validity in the immediate vicinity of the algebraic instability. However, the results strongly suggest that a 3D disk simulation will experience a significant dynamical response that, in all likelihood, will manifest itself as a finite amplitude phenomenon.

Because the equations describing Round Vortices are better posed (they retain all three time derivatives), their results are more indicative of the relative strength of the baroclinic instability. We saw that when the baroclinic effect was turned off (*i.e.* the lowest order linear solution) there was no linear instability, while when it was on there was a growth rate proportional to $t^{1/2}$. On the other hand, Rogers (1991) shows that sheared homogeneous flow (no rotation) in a sliding box frame is predicted to be linearly unstable with a growth rate that scales as $t \log t$ in the long time limit, much stronger than the instability predicted here. We view the relative weakness of the baroclinic instability to mean that instead of widespread turbulence the disk may support coherent structures in a way that is similar to organized large scale convection cells in atmospheres that only marginally exceed their critical Rayleigh numbers.

3. Dynamical structures of 2d jets in planetary vorticity fields

The following is a summary of work done in collaboration with N. J. Balmforth and C. Piccolo at the University of California, Santa Cruz, as presented in Balmforth, Piccolo & Umurhan, 2000 (BPU for short). We studied the stability and developed a reduced asymptotic model (a variant of the classical "single-wave model") for the 2D incompressible Bickley jet in a rotating planetary vorticity field (the β-plane). The Bickley jet profile in a planetary vorticity field has often been employed as a model to describe planetary scale jets like the Gulf Stream in the North Atlantic. The mathematical structure of the Bickley jet makes it relatively easy to develop asymptotically valid descriptions of the onset of coherent vortices, their shedding, and the generation of planetary scale jet meander. These asymptotic models also provide deeper insights into the dynamical differences between purely inviscid and nearly inviscid flows.

Sheehan *et al.* (1999) have proposed that protoplanetary disks may support jet flows that are similar to the jets observed on the outer cloud layers of Jupiter. If such strongly counterflowing jets do exist in the protoplanetary disk (and this would be borne out through numerical simulations), then it would not be a surprise if they also undergo a similar type of dynamical instability that are experienced by jets. A description of such disk jet instabilities by a reduced asymptotic model would be useful because it would provide a framework to study flow mixing and the cascade of the flow into increasingly complex structures. The work presented here for a simpler flow serves as a template for future endeavors in the context of exploring jet instabilities in protoplanetary disks.

Work in protoplanetary disks generally assumes inviscid flow since the viscosities appropriate for hydrogen and helium under typical disk temperatures predict Reynolds numbers on the order of 10^{12-14} (see BMU for details). Even if numerical simulations are attempted to reflect this nearly inviscid situation, as a practical matter some sort of artificial dissipation must be introduced in order to stabilize the schemes. However, the presence of viscosity may change the physical behavior of the flow from that of nearly or perfectly inviscid circumstances. Thus, it should be clearly understood what the differences are for nearly inviscid as opposed to totally inviscid flows since one assumption might predict dynamics different from the other.

3.1. *Problem formulation and linear theory*

We consider incompressible jet flow on a two-dimensional (x, y) plane. The plane is located in a rotating reference frame whose Coriolis parameter varies as a linear function of its planetary latitude (the β-plane), which is the y coordinate. In the following, all quantities have been non-dimensionalized by their appropriate length and time scale units. The equations governing the evolving portion of the fluid flow are,

$$\omega_t + U\omega_x + J(\psi, \omega) = \nu\nabla^2\omega + (U_{yy} - \beta)\omega_x \tag{3.1}$$

$$\psi_{xx} + \psi_{yy} = \omega, \tag{3.2}$$

where $\psi(x, y, t)$ and $\omega(x, y, t)$ denote the streamfunction and vorticity respectively. The quantity ν is the non-dimensionalized viscosity parameter, which is the inverse of the Reynolds number. The Bickley jet profile is given as $U(y) = \mathrm{sech}^2(y)$. Subscript y's and x's denote differentiation with respect to the y and x coordinate respectively. The nonlinear term J is $\psi_x\omega_y - \psi_y\omega_x$. The strength of the gradient of the planetary Coriolis parameter is given by β. For boundary conditions we choose periodic flow in x, and we find that the stability and evolution is insensitive to the boundary conditions in the y direction. For numerical purposes we require that the stream function be zero at some

suitably large value of $\pm y_0$, and for analytical purposes we require that the streamfunction be bounded as $y \to \pm\infty$.

Linear theory of Eqs. (3.1)–(3.2), which has been covered at least in part by others (*e.g.* Maslowe 1991 and Balmforth & Piccolo 2000), shows a number of interesting features. After assuming an $\exp i(kx - ct)$ solution form where k is the horizontal wavenumber and where c is the temporal eigenvalue, we find that the linear stability can be characterized by two parameters k and β. We refer the reader to Balmforth & Piccolo (2000) and BPU for details. Only some relevant highlights are discussed below.

The linear stability is qualitatively characterized by three regimes in the β-k^2 parameter plane: one in which Rossby waves propagate, one in which there exists a complex conjugate pair of modes (of which one is unstable) and one in which there is a continuous spectrum of eigenmodes. † The continuous spectrum occurs whenever the horizontal wavespeed is real and matches the flow speed, defining *the critical level*. The β-k^2 boundary for the continuous spectrum is where the critical level and the inflection point of the total flow (*i.e.* where $U_{yy} - \beta = 0$) coincide.

The parameter value pair $(\beta,k^2) = (-2, 6)$ is special because it represents the spot where all three dynamical regimes meet: much like a triple point in gaseous phase transitions. Physically, this parameter value represents the coincidence of the inflection point/critical-level at the jet tip. This special value of the parameter pair is where we develop an asymptotic description of the instability. It results in a variant of the *single-wave model* appearing often in plasma physics (Balmforth & Piccolo, 2000 and references therein).

3.2. *Results*

One of the challenges in deriving a weakly nonlinear description of the dynamics near the critical point (β,k^2) = (-2,6) is that the unstable mode that appears emerges out of the continuous spectrum. Standard center manifold type reductions of dynamical systems are successful because they exploit the fact that marginally unstable modes are isolated from other modes of the system. In this case, the emerging unstable mode comes from a continuum of modes, which in practice means that this continuum will also be excited as the system becomes unstable. In our analysis we take this effect into account (for details see BPU). The analysis considers small departures from the critical parameter value in powers of the small parameter ϵ,

$$\frac{\partial}{\partial t} \to -1 + \epsilon^2 \frac{\partial}{\partial T}, \qquad k^2 \to 6 + \epsilon\mu \qquad \beta \to -2 + \epsilon^2\beta_2, \qquad \nu \to \epsilon^4\nu_4, \tag{3.3}$$

and the streamfunction and vorticity have amplitudes scaled by ϵ^3. The analysis requires a number of matched asymptotic expansions relating the flow field away from the jet tip to the dynamics occurring in the tip region. The resulting nonlinear reduced model is expressed in terms of the scaled streamfunction and vorticity, Φ and Ω,

$$\Omega_T + Y^2\Omega_x + \Phi_x\Omega_Y = \lambda\Omega_{YY} - \kappa\Phi_T - \gamma\Phi_x \tag{3.4}$$

$$A \equiv \frac{1}{2\pi}\int_{-\pi}^{\pi} dx \int_{-\infty}^{\infty} dY e^{-ix}\Omega \qquad \text{and} \qquad \Phi = Ae^{ix} + c.c. \tag{3.5}$$

† By continuous spectrum we mean a collection of eigenmodes that have eigenfrequencies that are dense on a segment of the real axis.

where the coordinate x has been scaled by the the critical wavenumber $k_c = \sqrt{6}$. The departure parameters are,

$$\lambda = \nu_4/k_c, \qquad \kappa = 6/\mu, \qquad \gamma = 3\beta_2/4\mu. \tag{3.6}$$

Balmforth conducted numerical simulations of Eq. (3.1)–(3.2) to compare to the results of the reduced model Eq. (3.4)–(3.5) for values of the (unscaled) viscosity $\nu = 10^{-6}$. The agreement was exceptionally good, and the results were reported on at length in BPU. The reduced model predicted the onset and development of vortex structures at the tip of the jet in accordance with the numerical simulations.

Constructing a linear theory of the reduced set (assuming $\exp -i(cT + x)$ solutions) reveals subtle differences between the predictions of the nearly inviscid versus exactly inviscid flow. The first of these is that the predictions for the types of modes that propagate differs between the $\nu = 0$ and $\nu \to 0$ cases. The results are summarized in Fig. 2(a) and Fig. 3.

The $\nu = 0$ theory predicts that waves that are outside of the unstable regime (as depicted in Fig. 2) are neutrally stable. On the other hand, the $\nu > 0$ theory predicts that the eigenvalue c of at least one mode is approximately,

$$c \approx \frac{\lambda^{1/4} e^{-i\pi/8}}{\kappa}. \tag{3.7}$$

This predicts that those waves that are neutrally stable in the $\nu \to 0$ limit become viscously unstable if $k^2 < 6$ ($\mu < 0$) (see Fig. 4) and remain stable for $k^2 > 6$ ($\mu > 0$).

Another curious result of the inviscid versus nearly inviscid theory is that the inviscid theory predicts that there are either zero, one, or two modes of the system. In the nearly inviscid theory, in addition to the modes of the inviscid theory, there are a countably infinite number of viscous modes given by

$$c \approx (2n + 3/4)\sqrt{\lambda} e^{-i\pi/4}, \tag{3.8}$$

where n are the positive integers. For the problem at hand these modes are decaying and do not dynamically play an active role. However, in other problems they may possess different stability characteristics and one must be aware of their existence.

In summary, we have reduced the complicated dynamics of critical-layer/inflexion-point instabilities of a jet in a planetary vorticity field to a manageable set of asymptotic equations. The asymptotic validity of the equations was demonstrated, and we found that the reduced set offers a transparent view into some of the differences between assuming viscous versus inviscid flow. The methodology developed can be used in studying and dissecting the dynamics of other jet flows that might be manifest in protoplanetary disks.

4. Current directions

Current work with Barranco and Marcus is focused on developing a fully parallel three-dimensional spectral simulation of the Euler equations on an annular section of a Keplerian protoplanetary disk. We are preparing the simulation to be run on the SP2 Blue Horizon machine at the San Diego supercomputing center. The linear theory developed in § 2 will be used to provide checks for the code as it is developed. In addition, we have a number of analytical tasks that must be performed in support of the numerical simulations. These include the following:

- No analogous asymptotic expression for the energy content of the fluid has yet been developed. We must perform a similar analysis to the one performed in BMU in order to

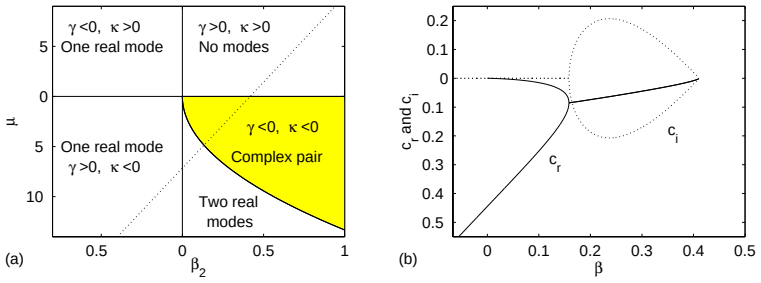

FIGURE 2. The types of propagating modes for the $\nu = 0$ theory. For $\beta_2 < 0$, all modes are neutral and they represent Rossby waves. In panel (b) we see the frequency and growth rates for the modes as a function along the dotted-line cut shown in panel (a). Note how the transition to instability occurs when the two real (Rossby) waves merge. c_r and c_i represent the real and imaginary parts of the eigenvalue.This

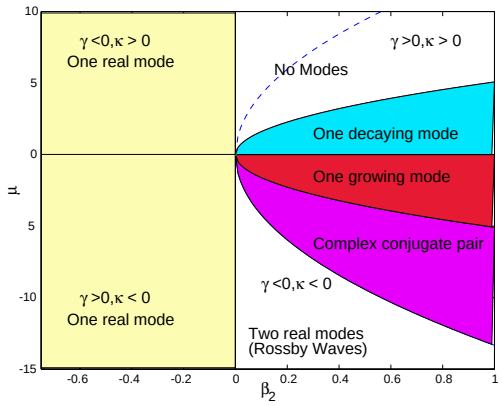

FIGURE 3. The $\nu \to 0$ limit of the viscous linear theory. The predictions should be compared to the $\nu = 0$ theory in Fig. 2. The types of modes that propagate as a function of parameter values are different between the two theories.

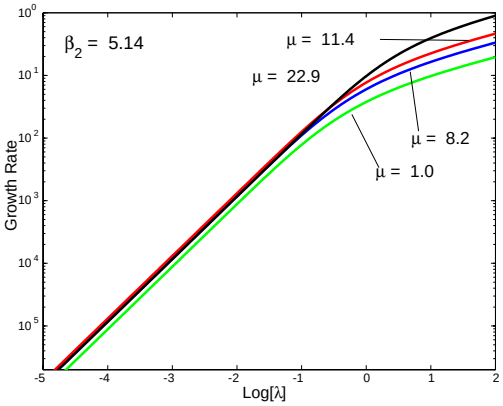

FIGURE 4. $\nu > 0$ tendency for $\beta_2 = -5.16$ for assorted values of μ. Whereas in the $\nu \to 0$ limit, the Rossby wave for this parameter regime is neutrally stable, the waves become viscously unstable when the viscosity is non-zero.

determine an asymptotically valid expression for a heat equation for the fluid. Analysis and judgments need to be made as to the relative time scales involved between the heating and cooling of the baroclinic disk against the time scales involved with the advected fluid fluctuations. Two extreme limits of the thermal time will yield an equation of state that is either isothermal or adiabatic.

- As seen throughout § 2, though baroclinicity induces some sort of instability in most cases, boundary conditions play a role in the onset criteria for instability of disturbances. Therefore, a detailed understanding of the implications of the various boundary conditions is required to judge whether or not the numerical simulations predict physically realizable phenomena. At the very least, interpretation of an instability will require an understanding of how the prescribed boundary conditions physically effect the flow and contribute to the instability.

Acknowledgment

I would like to thank Alan Wray for reading this manuscript and offering many scientific suggestions and numerical advice throughout the course of this and ongoing work.

REFERENCES

Barranco, J. & Marcus, P. S. & Umurhan, O. M. 2000 Scalings and Asymptotics of Coherent Vortices in Protoplanetary Disks. *Summer Program Proceedings*, Center For Turbulence Research, NASA Ames/Stanford Univ. 85-95.

Balbus, S. A. & Hawley, J. F. & Stone, J. M. 1996 Nonlinear stability, hydrodynamic turbulence, and transport in disks, *Astrophys. J.* **467**, 76-86.

Balmforth, N. & Piccolo, C. 2000 Onset of meandering in a baratropic jet. *J. Fluid Mech. in submission.*

Balmforth, N. & Piccolo, C. & Umurhan, O. 2000 Critical layer dynamics at the tip of a jet. *J. Fluid Mech. in submission.*

Bender, C. M. & Orszag, S. A. 1999 Advanced mathematical methods for scientists and engineers. Springer Verlag.

Chandresekhar, S. 1954 The instability of a layer of fluid heated below and subject to the simultaneous action of a magnetic field and rotation. I. *Astrophys. J.* **237**, 173-184.

Desch, S. 2000 Private communication.

Drazin, P. G. & Reid, W. H. 1982 Hydrodynamic Stability. Cambridge University Press.

Knobloch, E. & Spruit, H. C. 1986 Baroclinic waves in a vertically stratified thin disk. *Astron. Astrophys.* **166**, 359-367.

Marcus, P. S. 1984 Simulation of Taylor-Couette flow. II. Numerical results for wavy-vortex flow with one traveling wave. *J. Fluid Mech.* **146**, 65-113.

Marcus, P. S. 1993 Jupiter's Great Red Spot and other vortices. *ARAA* **31**, 523-573.

Marcus, P. S. & Press, W. H. 1977 Green's Functions for Small Disturbances of Plane Couette Flow. *J. Fluid Mech.* **79**, 525-534.

Marcus, P. S. & Tuckerman, L. S. 1987 Simulation of flow between concentric rotating spheres - Part II - Transitions, *J. Fluid Mech.* **185**, 31-66.

Marcy, G. W. & Butler, R. P. 1996 A planetary companion to 70 Virginis. *Astrophys. J.* **464**, L147-L151.

Maslowe, S.A. 1991 Baratropic instability of the Bickley jet. *J. Fluid Mech.* **266**, 417-426.

Perryman, MAC 2000 Extra-solar planets. *Reports on Progress in Physics.* **63**, 1209-1272.

Rogallo, R. S. 1981 Numerical experiments in homogeneous turbulence. *NASA Tech. Mem.* **81315**, 1-91.

Rogers, M. M. 1991 The structure of a passive scalar field with a uniform mean gradient in rapidly sheared homogeneous turbulent flow. *Phys. Fluids A.* **3**, 144-154.

Sheehan, D. P. & Davis, S. S. & Cuzzi, J. N. & Estberg, G. N. 1999 Rossby wave propagation and generation in the protoplanetary nebula. *Icarus.* **142**, 238-248.

Shu, F. A. & Johnstone, D. & Hollenbach, D. 1993 Photoevaporation of the solar nebula and the formation of the giant planets. *Icarus.* **106**, 92-101.